Probing Chirality of Crystals using Electron Paramagnetic Resonance (EPR) spectroscopy

Gil Otis
Bar Ilan University
Denial Aias
Bar Ilan University
Ilya Grinberg
Bar Ilan University
Sharon Ruthstein
Bar Ilan University
Yitzhak Mastai (mastai@biu.ac.il)
Bar Ilan University

Article

Keywords: Chirality, Electron paramagnetic resonance (EPR), Chiral crystals, chirality measurements

Posted Date: July 6th, 2022

DOI: https://doi.org/10.21203/rs.3.rs-1776678/v1

Abstract

One of the most challenging tasks in analytical chemistry is the determination of the chirality (identification of an enantio-meric composition) in solids mainly because of the strict requirements of the pharmaceutical industry for enantiomerically pure drugs. Although there are a few methods available to accomplish enantio-differentiation in solids, for example: X-ray diffraction (XRD), differential scanning calorimetry (DSC), CD spectroscopy, and low-frequency (LF) Raman spectroscopy, this is still very challenging. In this work, we have developed a new method to measure the chirality of crystals, based on electron paramagnetic resonance (EPR) spectroscopy of chiral crystals doped with Cu^{2+} as the EPR active ion. Here, we demonstrate our approach using a model system of L- and DL-Histidine crystals doped with Cu^{2+}. We show that EPR measurements of the Cu^{2+}-doped Histidine crystals can accurately determine the chirality and enantiomeric composition of the crystals. We present a very preliminary example of this technique, and we hope that in the future it will be possible to refine and develop this method for many other chiral organic crystal systems.

Introduction

Chirality is an important concept in both chemistry and biology, in particular, due to the chirality of most biological molecules, such as amino acids, sugars, proteins and nucleic acids. In the last few decades, the scientific importance of chiral substances led to developments in many areas such as the synthesis of enantiopure drugs, separation of enantiomers, and new techniques for identifying chiral molecules.[1–7] The most common techniques available at present to investigate chiral purity are based on measurement of chiral molecules in solution with optical techniques such as optical rotation (OR),[8,9] circular dichroism (CD),[10–12] vibrational circular dichroism (VCD),[13,14] Raman optical activity (ROA)[15,16] and high-performance liquid chromatography (HPLC).[17,18] However, in the solid-state, chirality measurements are considered challenging as there are only a few methods available, such as powder and single-crystal X-ray diffraction (XRD) analysis,[19,20] differential scanning calorimetry (DSC),[21] solid-state CD spectroscopy,[22,23] and low-frequency (LF) Raman spectroscopy.[24,25]

Chirality manifests itself in both molecules and crystals and recently there has been revived interest in the properties of chiral materials in the solid-state. Overall, there are three ways in which a chiral molecule can crystallize.[26] First, by forming a conglomerate crystal that is a mixture of well-resolved crystals of both enantiomers. Second, by forming racemic crystals containing the two enantiomers in an equal amount in the crystal unit cell. Finally, chiral systems can crystallize as enantiopure crystals that are composed of only one of the enantiomers in the crystal unit cell. It should be emphasized that the crystal unit cell of enantiomers and racemic compounds of the same chiral molecule are different, and this is the basis of the X-ray method's ability to probe chirality in crystals, however, accurate analysis of solid mixtures of enantiopure and racemic compounds by XRD is very limited due to peak overlapping and broadening, moreover, chiral analysis of mixtures of conglomerate and enantiopure crystals or mixtures

of two enantiopure crystals is impossible because they have the same diffraction pattern, emphasizing the need for novel methods for chiral analysis in powders.

In this paper, we present a new method for the investigation of chirality in crystals. Our method is based on the electron paramagnetic resonance (EPR) spectroscopy of chiral crystals doped with Cu^{2+} as the EPR active ion. The power of EPR lies in its ability to provide atomic-level information on paramagnetic metal ion (Cu^{2+}) coordination site With EPR spectroscopy, one can follow changes in the local environment of the paramagnetic species, represented by g-values, as well as changes in the interaction between the paramagnetic species and nearby nuclei such as ^{14}N nuclei (hyperfine coupling). [27–33]

Here, we have chosen Histidine crystals as a model system for chiral crystallization. Enantiopure crystals of L-His crystallize in a monoclinic unit cell with a space group of P 2_1 (or the orthorhombic unit cell with a space group of P 2_1 2_1 2_1).[34] The racemic crystals of DL-His crystallize in a monoclinic form with a space group of P $2_1/c$.[35] As explained above, our method is based on the use of chiral crystals doped with minute amounts of Cu^{+2} ions.

Results

Crystallization and characterization of chiral crystals

Cu^{2+}-doped pure L-Histidine crystals were prepared by the slow evaporation method.[36] Generally, 2 g of L-Histidine were mixed with 8.7 mg of $CuCl_2$ (0.5% mol) and dissolved in 30 mL of dilute HCl solution (pH = 2.7). The turbid solution was carefully heated until it reached complete dissolution. It was then left to cool to room temperature and kept for four days to crystallize. The same procedure was followed for the DL-Histidine crystals except that 1 g of L-Histidine and 1 g of D-Histidine were mixed. After four days, the Cu^{2+}-doped crystals of L-His or DL-His were collected using a Büchner funnel and washed several times with water and ethanol. The Cu^{2+}-doped Histidine crystals were then dried under vacuum and characterized. The crystalline structure of Cu^{2+}-doped Histidine is not reported in the literature, and so we performed density functional theory (DFT) calculations to find the coordination complexes of Cu in the L- and DL-crystalline structures. The structures of L-His and DL-His (80-atom unit cells) with an added Cu^{2+} ion (for a total of 81 atoms) were allowed to relax in order to find the minimum energy structure through the optimization of the lattice parameters and the internal positions of the atoms within the unit cell. The total energy was converged with respect to both the kinetic energy cutoff and k-point sampling for both structures. The kinetic energy cutoff was 40 Ry, and the gamma k-point grid was used for the calculations. In Fig. 1, the location and coordination of Cu^{+2} in L- and DL-His crystals are shown.

In both the L- and DL-His crystals, the Cu^{2+} ion is coordinated with six chemical groups of nitrogen, oxygen, and carbon. However, in each crystalline structure, the distances and geometry of the copper from the chemical groups are different (see Table S2, SI). Pure L-His crystals are known to crystalize in two different polymorphs (form A and form B).[31] Form A is monoclinic with a space group of P 2_1 and

form B is orthorhombic with a space group of P 2_1 2_1 2_1. Under regular aqueous crystallization conditions, the two forms are usually in equilibrium and both of them precipitate.[34, 37,38] In our case, probably due to the incorporation of copper in the crystal lattice, the majority of the crystals crystalize in form A. This effect was also shown with $NaBF_4$ doped L-His crystals.[39] The diffraction peaks that are associated with the B-form crystals are marked with an asterisk in the diffraction graph of Cu^{2+}-doped L-His crystals (Fig. 2). DL-His crystals are known to crystalize only in the monoclinic form of DL-His with a space group of P $2_1/c$[32], and so the Cu^{2+}-doped DL-His crystals were found to have the same form, as shown in Fig. 2.

Differential scanning calorimetry (DSC) was used to examine the thermodynamic properties of the crystals. The endothermic peak at around 260 ^oC that occurs in all the crystals is attributed to water loss from the histidine crystal.[39,40] In the literature This reaction was reported to take place at around 275 ^oC.[40] We believe that the difference in the results is due to copper doping of the crystal. Cu^{2+}-doped L-His crystals have a transition temperature of 265.5 ^oC while the Cu^{2+}-doped DL-His crystals have a transition temperature of 262 ^oC (Fig. 2), the FTIR spectra of Cu^{2+}-doped L and DL-His is presented in figure S1 (SI), Cu^{2+} concentrations (ppm) inside the L and DL-His crystals were measured by ICP and given in table S1 (SI).

Chirality Measurements Of Chiral Crystals With Epr

In the next phase of this study, we verified the ability of EPR spectroscopy to probe the chirality of the L- and DL-His crystals. To do this, we prepared different dry crystal powders mixtures of Cu^{2+}-doped L- and DL-His. The dry crystals of Cu^{2+}-doped L and DL-His crystals were weighed very accurately and mixed in different ratios: 50%L/50%DL, 60%L/40%DL, and so on. The mixtures were analyzed by EPR spectroscopy.

The coordination site of Cu^{2+} was characterized by echo-detected field sweep EPR measurements and electron spin echo envelope modulation (ESEEM) pulsed EPR experiments. Field sweep EPR measurements can determine the number of ^{14}N nuclei directly coordinated to Cu^{2+}.[28] ESEEM experiments, on the other hand, detect the anisotropic hyperfine interaction between Cu^{2+} and ^{14}N nuclei that are not directly bound to the paramagnetic metal ion, but are situated nearby (within 2–6 Å).[29,41] EPR Q-band spectra at 20K were acquired for all crystals, were then derived, and were analyzed using EasySpin simulation package[42] (see Figure S3, SI). The spectra were fitted with three species having axial symmetry, and the g and the hyperfine tensors were evaluated. These parameters can provide information on the direct nuclei coordination around the Cu^{2+} ion. For the DL-crystal, the data fitted with one dominant species, which according to Peisach and Blumberg[28] suggests 3O1N coordination. The L-crystal data were fitted with three species, with 20% 3O1N coordination, and 80% 3N1O or 4N coordination (see Table S3, SI). The extent of the “DL species” in each crystal was evaluated and plotted in Fig. 3I. When

increasing the L-His concentration in the crystal, we observed a higher amount of directly coordinated ^{14}N nuclei.

As a simple control experiment, all the L- and DL-crystal mixtures (1 mg powder) were dissolved in concentrated hydrochloric acid and diluted tenfold. The solutions were then measured by CD spectroscopy, and the enantiomeric excess (e.e.) of L-His was calculated in each sample and compared to the theoretical e.e. value (see Figure S4, SI). Interestingly, the fit between the theoretical and the measured data in the CD measurements (R^2 = 0.8933) was a little poorer than that of the EPR measurements (R^2 = 0.9317).

Next, ESEEM experiments were performed in order to measure the interaction of the electron spin of Cu^{2+} with nearby ^{14}N (∼2–6 Å) nuclei. These nuclei are typically not directly coordinated to the metal ion but lie on the residue that is directly bonded to the metal ion. The Fourier transform spectrum of the ESEEM signal of ^{14}N nuclei is usually characterized by a narrow characteristic component between 0–3 MHz. The intensity of this line is directly related to the number of ^{14}N nuclei within the environment of Cu^{2+}. We measured the intensity at 2.8 MHz for the various crystals (Fig. 3**II**) and detected an increase in the intensity with increase in L-His concentration, which is in agreement with the CW-EPR data.

The DFT calculations (see Table S2, SI) suggest that the closest nuclei to Cu^{2+} ion in the DL-crystal are three oxygen atoms (at distances 2.07, 3.07 and 3.87 Å) and two nitrogen atoms (3.32, 3.64 Å), whereas in the L-crystal there are two very close oxygen nuclei (2.05, 2.1 Å) and two close nitrogen nuclei (3.16, 3.17 Å). The magnetic values derived from the field sweep EPR spectra are affected by the nearby nuclei (i.e. ^{14}N) around the Cu^{2+} ion. These nuclei influence the spin density around the Cu^{2+} leading to changes in the g-tensor and hyperfine values. Increase of ^{14}N nuclei around the Cu^{2+} leads to reduction in the g-tensor and hyperfine parallel values (parallel to the magnetic field).[27, 28, 45] This agrees with the DFT results which shows that the ^{14}N nuclei are closer to the Cu^{2+} ion in the L-crystal than in the DL-crystal. Moreover, the ESEEM experiments, which are sensitive to distant ^{14}N nuclei in the imidazole ring, confirmed the presence of nearby imidazole rings in the L-crystals. However, while there is nice agreement between the EPR and DFT data of the DL-crystal, suggesting that the most probable coordination for Cu^{2+} ion is 3O1N coordination (see Figure S2. SI), there is some disagreement regarding the L-crystals. The EPR data suggests a greater number of ^{14}N nuclei around the Cu^{2+} ion in the L-crystal (3–4 ^{14}N nuclei), while the DFT data found only two nearby ^{14}N nuclei. However, the DFT calculations suggest a more packed environment for the L-crystals, which might lead to the changes detected by the EPR experiments. While DFT calculations are performed on a small supercell, the EPR experiments are conducted on a powder of crystals, possibly leading to some disagreement. Overall, the use of both field sweep EPR and ESEEM experiments allowed us to differentiate between various chiral crystals. The identification of racemic or chiral crystals is crucial for many applications. Currently, several methods allow racemic crystals to be distinguished from enantiopure crystals. These include SHG-CD, X-ray diffraction, LW-Raman among others. However, each method has its advantages and disadvantages.

Chirality Measurements Of Additional Chiral Crystals

In addition, our novel method of monitoring the chirality of crystals by EPR measurements was also demonstrated on two other chiral crystal systems; one, sodium chlorate (NaClO3) chiral crystals, these crystals were used in one of the earliest experiments on chiral induction in naturally chiral inorganic crystals, in the famous experiments[43], chiralsymmetry breaking was achieved through continueus stirring of the solution during crystallization, the stirred product was almost enantiomerically pure (99.7%) while the non-stirred product was racemic. we crystalized the pure enantiomer and the racemic conglomerate with Cu^{+2} doping and were able to distinguish between the homochiral and the conglomerate crystals using EPR measurements (Fig. 4I). The second chiral system we tested is a copper iodide complex of the well-known BINAP molecule (R/S-$[Cu(binap)I]_2$) which displays axial chirality[44], we crystalized the R and S copper iodide complexes and proved the ability of EPR to differentiate between two homochiral crystals (Fig. 4II). The diffraction patterns of all the materials were taken it was not possible to measure the crystal chirality based on the diffraction (see Figures S5 and S6, SI).

Conclusions

In this article, we add a new method to our “analytical toolbox” to identify the chirality of crystals and solids. The method is based on electron paramagnetic resonance (EPR) spectroscopy of chiral crystals doped with an EPR active ion as Cu^{2+}. It is well- known that the unit cell and crystal structures of racemic and chiral crystals are different. By adding Cu^{2+} ions to these crystal structures, we can use EPR to determine the short-range order and the molecular environment of the Cu^{2+} in the solids and, hence, the chirality of the crystals. Here, we have demonstrated this for the case of L- and DL-His crystals and have shown that this method has a high sensitivity for chiral identification of solid mixtures, we have also demonstrated the use of EPR to distinuigsh between conglometrate and homochiral crystals in the case of $NaClO_3$, and to distinguish between two homochiral crystals in the case of R/S-$[Cu(binap)I]_2$.

This work gives a very preliminary example of the technique, and we hope that in the future it will be possible to refine and develop this method using other metal ions and many other chiral organic crystals systems. For many years, scientists have been investing efforts in the development of new methods for analyzing and identifying chirality in the solid-state. We believe that the method we propose in this article will expand the range of methods for chiral analysis in crystals, and will be developed and applied by many others.

Methods

Materials. L and D-Histidine (99%, HPLC) were purchased from TCI EUROPE N.V., Copper chloride dihydrate, (R)−BINAP, (S)−BINAP, Copper (I) iodide 98%, and Sodium chlorate were purchased from sigma Aldrich Co 3050 Spruce Street. St Louis USA Ethanol absolute was purchased from Bio-Lab Ltd, Hayetzira Jerusalem Israel, hydrochloric acid 37% was purchased from DAEJUNG Co, Ltd.

Experimental conditions. The crystallographic structure of the L and DL-His crystals was measured by X-ray diffraction (XRD), measurements were performed using a Bruker AXS D8 Advance diffractometer with Cu Ka (λ = 1.5418 Å) operating at 40 kV/40 mA, and collecting from 2θ = 10° to 80°, DSC measurements were performed with a Mettler Toledo model DSC 822e equipped with a liquid-nitrogen cooling accessory and calibrated with indium, Samples were heated from 30 to 350°C at 2°C/min under N_2 flow, FTIR spectrum was collected using a Thermo Scientific Nicolet iS10 FTIR spectrometer equipped with a Smart iTR attenuated total reflectance sampler containing a single bounce diamond crystal. Data were collected and analyzed using OMNIC software. Spectra were collected in the 650–4000 cm-1 range at a spectral resolution of 4, Copper concentrations inside the crystals was measured using Inductive Coupled Plasma (ICP). Measurements were taken using a SPECTRO ARCOS ICP-OES Multi view FHX22 instrument, powder samples (3 mg) were dissolved in concentrated hydrochloric acid and diluted with distilled water to a final acid concentration of 3 weight %. CD measurments were done using a Chirascan spectrometer (Applied Photophysics, UK) at room temperature. Measurements were carried out in a 1 cm optical path length cell and the data were recorded from 200–260 nm with a step size and a bandwidth of 1 nm. Spectra were obtained after background subtraction.

Computational detailes. All electronic structure calculations were done using density functional theory with the Perdew-Burke-Ernzerhof (PBE) exchange-correlation functional and ultrasoft pseudopotentials using the Quantum Espresso software package. The ultrasoft pseudopotentials are taken from the Rutgers university GBRV database.[46] In the self-consistent calculations, the energy was converged below 10–8 Ry and the force convergence criteria is set to 10–5 a.u.

EPR measurments. Q-band spectra were recorded with Elexsys E580 at 20 K, using a two-pulse echo field sweep experiment with a π pulse of 24 ns, and a tau value of 200 ns, the repetition time was 5 ms. The frequency was 33.86 GHz. The presented spectra are derivatives of the absorption field sweep spectra. The samples were measured in 1.6 mm quartz tubes (Wilmad-LabGlass, Vineland, NJ, USA).

ESEEM experiments. A $\pi/2$-τ-$\pi/2$-T + dt-$\pi/2$-τ-echo sequence was used with a four-step phase. Q-band measurements at Elexsys E580 equipped with 50W AmpQ. The measurements were performed at 33.86 GHz, 11790 G, at 20K. The $\pi/2$ pulse length was 12 ns and the data was acquired with τ set of 220 ns to amplify ^{14}N modulations. The initial T was 80 ns. The data was processed by subtracting the baseline using a polynomial fit. The resulting time domain was convoluted with a hamming window function, and the spectrum obtained by cross-term averaging Fourier transform.

Crystallization of Cu-doped $NaClO_3$ chiral crystals. The crystallization of Cu-doped $NaClO_3$ chiral crystals was done according to a procedure that is very well known in the literature, one of the most famous works on chiral crystals is the crystallization of $NaClO_3$ crystals under continues stirring, it was shown, that preforming the crystallization without stirring gave a racemic conglomerate of both L and D crystals, however, when the solution is stirred almost all of the crystals (99.7%) formed in the same chirality either L or D crystals[47].

In our experiments we have reproduced the exact crystallization method[3] with the only difference being the doping by Cu ions to allow the EPR measurements. Briefly, two samples, each containing 6.25 gr of $NaClO_3$ and 4 mg of $CuCl_2$ (0.5% mol) were each dissolved in 7.5 mL of DDW, the samples were mildly heated (50–60 ^{0}C) until the solution became clear, next, the solutions were cooled down to room temp and kept for 1 week at room temp for the crystallization process, one sample was continuously stirred while the other one was not, after one week, the crystals were collected, filtered and washed several times with ethanol and dried under vacuum. The crystals were then milled to a fine powder and the powders were taken to XRD and EPR measurements.

Precipitation of R/S – [Cu(binap)I] $_2$ chiral complexes. The Precipitation of the chiral complexes was conducted according to a published procedure[48], briefly, 311 mg of R/S – BINAP and 95 mg of CuI were dissolved by 10 mL of acetonitrile under N_2 atmosphere, the solution was kept for 1 hour with continues stirring in room temp to produce the R/S - $[Cu(binap)I]_2$ complexes which precipitated to give yellow powders. The powders were then filtered and washed several times with ethanol and finally dried under vacuum. The dry powders were taken to XRD and EPR measurements.

Declarations

ASSOCIATED CONTENT

FTIR spectra of Cu^{2+}-doped L-His and DL-His crystals, Cu^{2+} concentrations measured by inductive coupled plasma (ICP), Distances between the Cu^{2+} ion and nearby atoms derived from the DFT calculations, EPR spectra and simulated EPR spectra for powder mixtures, Simulated EPR parameters using easyspin program, CD spectra of mixtures of Cu^{2+}-doped L-His and DL-His, Diffraction pattern of Cu^{2+}-doped NaClO3 chiral crystals, and Diffraction pattern of R/S – $[Cu(binap)I]_2$ chiral complexes (**PDF**).

AUTHOR INFORMATION

Corresponding Author

* **Prof. Yitzhak Mastai -** Department of Chemistry and Institute for Nanotechnology and Advanced Materials, Bar-Ilan University Ramat Gan 5290002, Israel. E-mail: Yitzhak.Mastai@biu.ac.il

* **Prof. Sharon Ruthstein -** Department of Chemistry, Bar-Ilan University Ramat Gan 5290002, Israel. E-mail: sharon.ruthstein@biu.ac.il

Authors

Gil Otis - Department of Chemistry and Institute for Nanotechnology and Advanced Materials, Bar-Ilan University Ramat Gan 5290002, Israel. E-mail: gotis89@gmail.com

Denial Aias - Department of Chemistry, Bar-Ilan University Ramat Gan 5290002, Israel. E-mail: denial.aias@gmail.com

Prof. Ilya Grinberg - Department of Chemistry, Bar-Ilan University Ramat Gan 5290002, Israel. E-mail: ilya.grinberg@biu.ac.il

Funding Sources

This research was supported by the Israel Science Foundation (ISF) (Grant No. 2546/21).

Notes

The authors declare no competing financial interest.

ACKNOWLEDGMENT

Gil Otis acknowledges the Bar-Ilan President's Ph.D. Scholar and the Institute for Nanotechnology and Advanced Materials at Bar-Ilan University for Ph.D. Scholarship.

References

1. Huang, X.Y.; Pei, D.; Liu, J. F.; Di, D. L., A review on chiral separation by counter-current chromatography: Development, applications and future outlook. Journal of Chromatography A 2018, *1531*, 1–12.
2. Liu, T.; Li, Z.; Wang, J.; Chen, J.; Guan, M.; Qiu, H., Solid membranes for chiral separation: A review. Chemical Engineering Journal 2020, 128247.
3. Schmid, M. G.; Hägele, J. S., Separation of enantiomers and positional isomers of novel psychoactive substances in solid samples by chromatographic and electrophoretic techniques–A selective review. Journal of Chromatography A 2020, *1624*, 461256.
4. Matsumoto, A.; Kaimori, Y.; Uchida, M.; Omori, H.; Kawasaki, T.; Soai, K., Achiral inorganic gypsum acts as an origin of chirality through its enantiotopic surface in conjunction with asymmetric autocatalysis. Angewandte Chemie International Edition **2017**, *56* (2), 545–548.
5. Wojaczyńska, E. b.; Wojaczyński, J., Modern stereoselective synthesis of chiral sulfinyl compounds. Chemical reviews **2020**, *120* (10), 4578–4611.
6. Zhao, Y.; Askarpour, A. N.; Sun, L.; Shi, J.; Li, X.; Alù, A., Chirality detection of enantiomers using twisted optical metamaterials. Nature communications **2017**, *8* (1), 1–8.
7. Baykusheva, D.; Zindel, D.; Svoboda, V.; Bommeli, E.; Ochsner, M.; Tehlar, A.; Wörner, H. J., Real-time probing of chirality during a chemical reaction. *Proceedings of the National Academy of Sciences* **2019**, *116* (48), 23923–23929.
8. Ishikawa, K.; Tanaka, M.; Suzuki, T.; Sekine, A.; Kawasaki, T.; Soai, K.; Shiro, M.; Lahav, M.; Asahi, T., Absolute chirality of the γ-polymorph of glycine: correlation of the absolute structure with the optical

rotation. Chemical Communications **2012**, *48* (48), 6031–6033.

9. Li, D.; Guan, T.; Liu, F.; Yang, A.; He, Y.; He, Q.; Shen, Z.; Xin, M., Optical rotation based chirality detection of enantiomers via weak measurement in frequency domain. Applied Physics Letters 2018, *112* (21), 213701.
10. Gottarelli, G.; Lena, S.; Masiero, S.; Pieraccini, S.; Spada, G. P., The use of circular dichroism spectroscopy for studying the chiral molecular self-assembly: an overview. Chirality: The Pharmacological, Biological, and Chemical Consequences of Molecular Asymmetry **2008**, *20* (3-4), 471–485.
11. Vorlíčková, M.; Kejnovská, I.; Bednářová, K.; Renčiuk, D.; Kypr, J., Circular dichroism spectroscopy of DNA: from duplexes to quadruplexes. Chirality 2012, *24* (9), 691–698.
12. Wolf, C.; Bentley, K. W., Chirality sensing using stereodynamic probes with distinct electronic circular dichroism output. Chemical Society Reviews 2013, *42* (12), 5408–5424.
13. Joyce, L. A.; Nawrat, C. C.; Sherer, E. C.; Biba, M.; Brunskill, A.; Martin, G. E.; Cohen, R. D.; Davies, I. W., Beyond optical rotation: what's left is not always right in total synthesis. Chemical science 2018, *9* (2), 415–424.
14. Freedman, T. B.; Cao, X.; Dukor, R. K.; Nafie, L. A., Absolute configuration determination of chiral molecules in the solution state using vibrational circular dichroism. Chirality 2003, *15* (9), 743–758.
15. Mensch, C.; Konijnenberg, A.; Van Elzen, R.; Lambeir, A. M.; Sobott, F.; Johannessen, C., Raman optical activity of human α-synuclein in intrinsically disordered, micelle-bound α-helical, molten globule and oligomeric β-sheet state. Journal of Raman Spectroscopy **2017**, *48* (7), 910–918.
16. Wu, T.; Li, G.; Kapitan, J.; Kessler, J.; Xu, Y.; Bouř, P., Two Spectroscopies in One: Interference of Circular Dichroism and Raman Optical Activity. Angewandte Chemie 2020, *132* (49), 22079–22082.
17. Lidor-Shalev, O.; Pliatsikas, N.; Carmiel, Y.; Patsalas, P.; Mastai, Y., Chiral metal-oxide nanofilms by cellulose template using atomic layer deposition process. ACS nano **2017**, *11* (5), 4753–4759.
18. Ward, T. J.; Ward, K. D., Chiral separations: fundamental review 2010. Analytical chemistry **2010**, *82* (12), 4712–4722.
19. Flack, H.; Bernardinelli, G., The use of X-ray crystallography to determine absolute configuration. Chirality: The Pharmacological, Biological, and Chemical Consequences of Molecular Asymmetry 2008, *20* (5), 681–690.
20. Crasto, D.; Malola, S.; Brosofsky, G.; Dass, A.; Häkkinen, H., Single crystal XRD structure and theoretical analysis of the chiral Au30S (S-t-Bu) 18 cluster. Journal of the American Chemical Society 2014, *136* (13), 5000–5005.
21. Medina, D. D.; Goldshtein, J.; Margel, S.; Mastai, Y., Enantioselective crystallization on chiral polymeric microspheres. Advanced Functional Materials 2007, *17* (6), 944–950.
22. Bilotti, I.; Biscarini, P.; Castiglioni, E.; Ferranti, F.; Kuroda, R., Reflectance circular dichroism of solid-state chiral coordination compounds. Chirality: The Pharmacological, Biological, and Chemical Consequences of Molecular Asymmetry 2002, *14* (9), 750–756.

23. Zheng, Y.; Lin, L.; Ye, X.; Guo, F.; Wang, X., Helical graphitic carbon nitrides with photocatalytic and optical activities. Angewandte Chemie 2014, *126* (44), 12120–12124.
24. Aviv, H.; Nemtsov, I.; Mastai, Y.; Tischler, Y. R., Characterization of crystal chirality in amino acids using low-frequency Raman spectroscopy. The Journal of Physical Chemistry A **2017**, *121* (41), 7882–7888.
25. Nemtsov, I.; Mastai, Y.; Tischler, Y. R.; Aviv, H., Chiral Purity of Crystals Using Low-Frequency Raman Spectroscopy. *ChemPhysChem* 2018, *19* (22), 3116–3121.
26. Jacques, J.; Collet, A.; Wilen, S. H., *Enantiomers, racemates, and resolutions*. Wiley: 1981.
27. Aronoff-Spencer, E.; Burns, C. S.; Avdievich, N. I.; Gerfen, G. J.; Peisach, J.; Antholine, W. E.; Ball, H. L.; Cohen, F. E.; Prusiner, S. B.; Millhauser, G. L., Identification of the Cu^{2+} binding sites in the N-terminal domain of the prion protein by EPR and CD spectroscopy. Biochemistry 2000, 13760–13771.
28. Peisach, J.; Blumberg, W. E., Structural implications derived from the analysis of electron paramagnetic resonance spectra of natural and artificial copper proteins. Arch. Biochem. Biophys. 1974, *165*, 691–708.
29. Ruthstein, S.; Stone, K. M.; Cunningham, T. F.; Ji, M.; Cascio, M.; Saxena, S., Pulsed Electron Spin Resonance resolves the coordination site of Cu^{2+} ions in a1-Glycine receptor. Biophysical Journal 2010, *99*, 2497–2506.
30. Shenberger, Y.; Marciano, O.; Gottlieb, H.; Ruthstein, S., Insights into the N-terminal Cu(II) and Cu(I) binding sites of the human copper transporter CTR1. J. Coord. Chem. 2018, *71*, 1985–2002.
31. Stegmann, H. B.; Mäurer, M.; Höfler, U.; Scheffler, K.; Hewgill, F., Chiral recognition by 1H-NMR, EPR, and ENDOR spectroscopy. Chirality 1993, 5(4), 282–287.
32. Schuler, P.; Schaber, F. M.; Stegmann, H. B.; Janzen, E., Recognition of chirality in nitroxides using EPR and ENDOR spectroscopy. Magnetic resonance in chemistry 1999, 37(11), 805–813.
33. Otis, G.; Nassir, M.; Zutta, M.; Saady, A.; Ruthstein, S.; Mastai, Y., Enantioselective crystallization of chiral inorganic crystals of ϵ-Zn (OH) 2 with amino acids. Angewandte Chemie 2020, 132(47), 21110–21115.
34. Wantha, L.; Punmalee, N.; Sawaddiphol, V.; Flood, A. E., Effect of Ethanol on Crystallization of the Polymorphs of L-Histidine. Journal of Crystal Growth 2018, *490*, 65–70.
35. Edington, P.; Harding, M. M., The crystal structure of DL-histidine. Acta Crystallographica Section B: Structural Crystallography and Crystal Chemistry 1974, *30* (1), 204–206.
36. He, G.; Bhamidi, V.; Wilson, S. R.; Tan, R. B.; Kenis, P. J.; Zukoski, C. F., Direct growth of γ-glycine from neutral aqueous solutions by slow, evaporation-driven crystallization. Crystal growth & design 2006, *6* (8), 1746–1749.
37. Ravanfar, R.; Abbaspourrad, A., l-Histidine Crystals as Efficient Vehicles to Deliver Hydrophobic Molecules. ACS applied materials & interfaces 2019, *11* (42), 39376–39384.
38. Novelli, G.; Maynard-Casely, H. E.; McIntyre, G. J.; Warren, M. R.; Parsons, S., Effect of High Pressure on the Crystal Structures of Polymorphs of l-Histidine. Crystal Growth & Design 2020, *20* (12), 7788–

7804.
39. Syamala, D.; Rajendran, V.; Natarajan, R.; Babu, S. M., Effect of sodium fluoroborate ($NaBF_4$) doping on the NLO properties of L-histidine single crystals. Crystal growth & design 2007, *7* (9), 1695–1698.
40. Shibata, F.; Yokota, M.; Doki, N., Thermodynamic characteristics of L-histidine polymorphs and effect of ethanol on the crystallization. Journal of Crystal Growth 2021, *564*, 126086.
41. Stenland, C.; Kevan, L., Electron-Spin-Resonance and Electron-Spin Echo Modulation Studies of the Photoionization of N-Alkyl-N,N',N'-Trimethylbenzidines in Anionic, Zwitterionic, and Cationic Vesicles - Correlation of Photoproduced Cation Location with the Photoyield. Langmuir 1994, *10* (4), 1129–1133.
42. Stoll, S.; Schweiger, A., EasySpin, a Comprehensive Software Package for Spectral Simulation and Analysis in EPR. J. Magn. Reson. 2006, *178* (1), 42–55.
43. Kondepudi, D. K.; Kaufman, R. J.; Singh, N., Chiral symmetry breaking in sodium chlorate crystallization. Science. 1990, 250(4983), 975–976.
44. Xu, Z., Yu, X.; Sang, X.; Wang, D., BINAP-copper supported by hydrotalcite as an efficient catalyst for the borrowing hydrogen reaction and dehydrogenation cyclization under water or solvent-free conditions. Green Chemistry. 2018, 20(11), 2571–2577.
45. Chattopadhyay, M.; Walter, E. D.; Newell, D. J.; Jackson, P. J.; Aronoff-Spencer, E.; Peisach, J.; Gerfen, G. J.; Bennett, B.; Antholine, W. E.; Millhauser, G. L., The octarepeat domain of the prion protein binds Cu(II) with three distinct coordination modes at pH 7.4. J. Am. Chem. Soc. 2005, *127*, 12647–12656.
46. Garrity, K. F.; Bennett, J. W.; Rabe, K. M.; Vanderbilt, D., Pseudopotentials for high-throughput DFT calculations. Computational Materials Science 2014, *81*, 446–452.
47. Kondepudi, D. K.; Kaufman, R. J.; Singh, N., Chiral symmetry breaking in sodium chlorate crystallizaton **1990**, Science, *250*(4983), 975–976.
48. Xu, Z.; Yu, X.; Sang, X.; Wang, D., BINAP-copper supported by hydrotalcite as an efficient catalyst for the borrowing hydrogen reaction and dehydrogenation cyclization under water or solvent-free conditions. Green Chemistry 2018, *20*(11), 2571–2577.

Figures

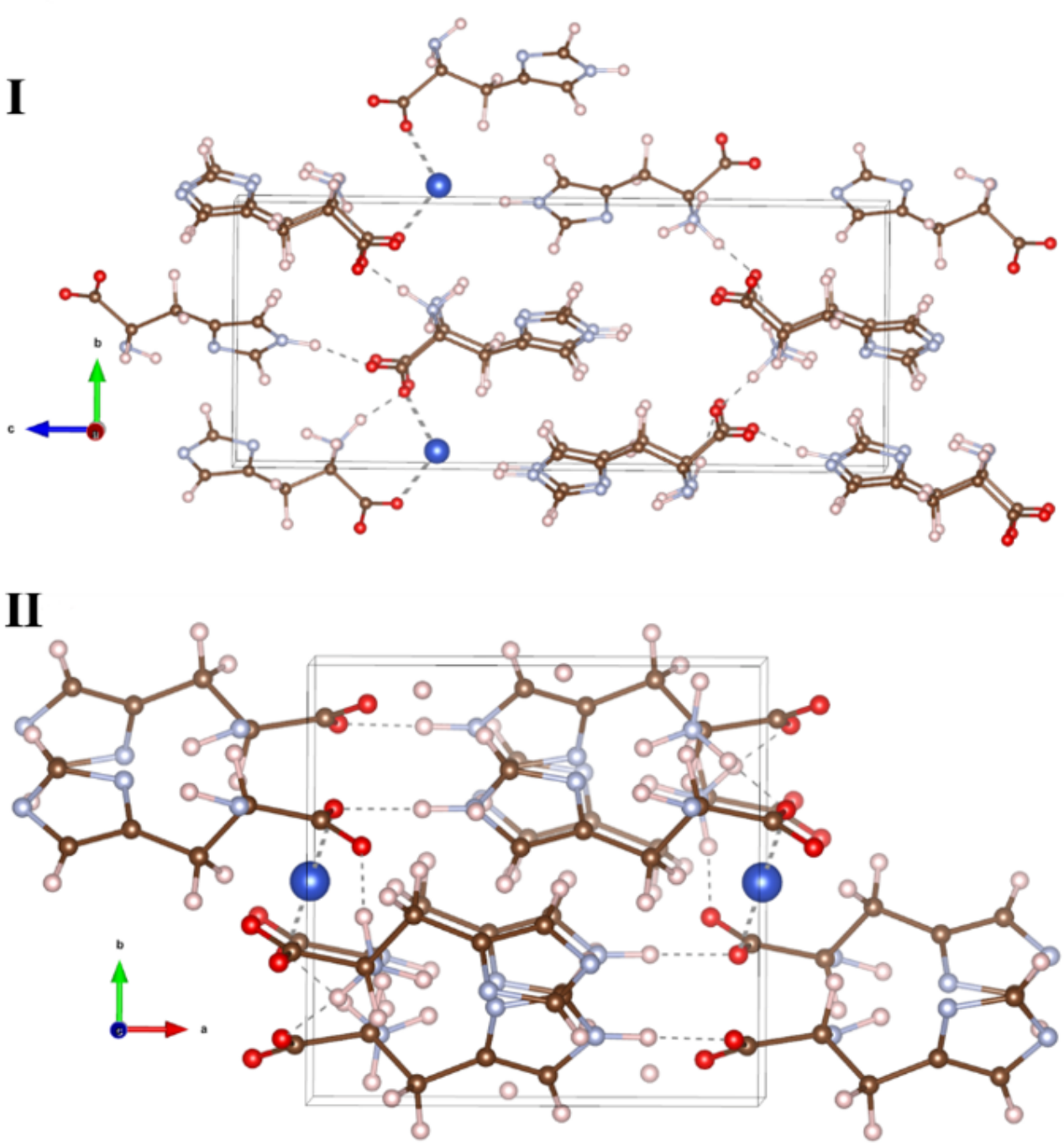

Figure 1

Crystal structures of Cu^{2+}-doped L/DL-His crystals: DFT calculations of Cu^{2+}- doped L-His (**I**) and DL-His (**II**) crystals. The unit cell in each crystal structure is highlighted, red atoms represent oxygen, light blue represents nitrogen, brown represents carbon and dark blue represents copper.

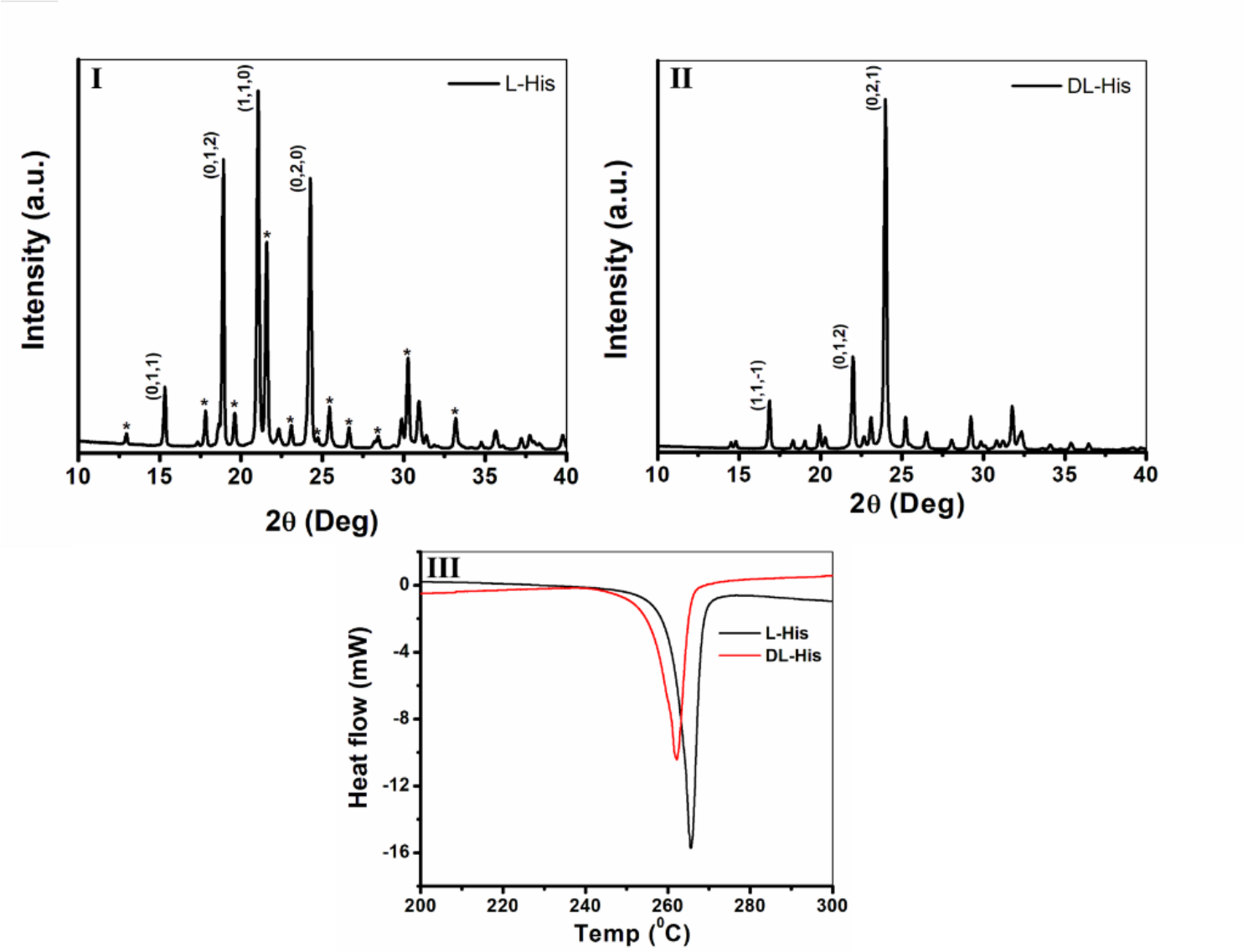

Figure 2

Characterization of Cu^{2+}-doped L/DL-His crystals: XRD graph of Cu^{2+}-doped L-His crystals (**I**) and Cu^{2+}-doped DL-His racemate crystals (**II**), DSC of Cu-doped L/DL-His crystals (**III**).

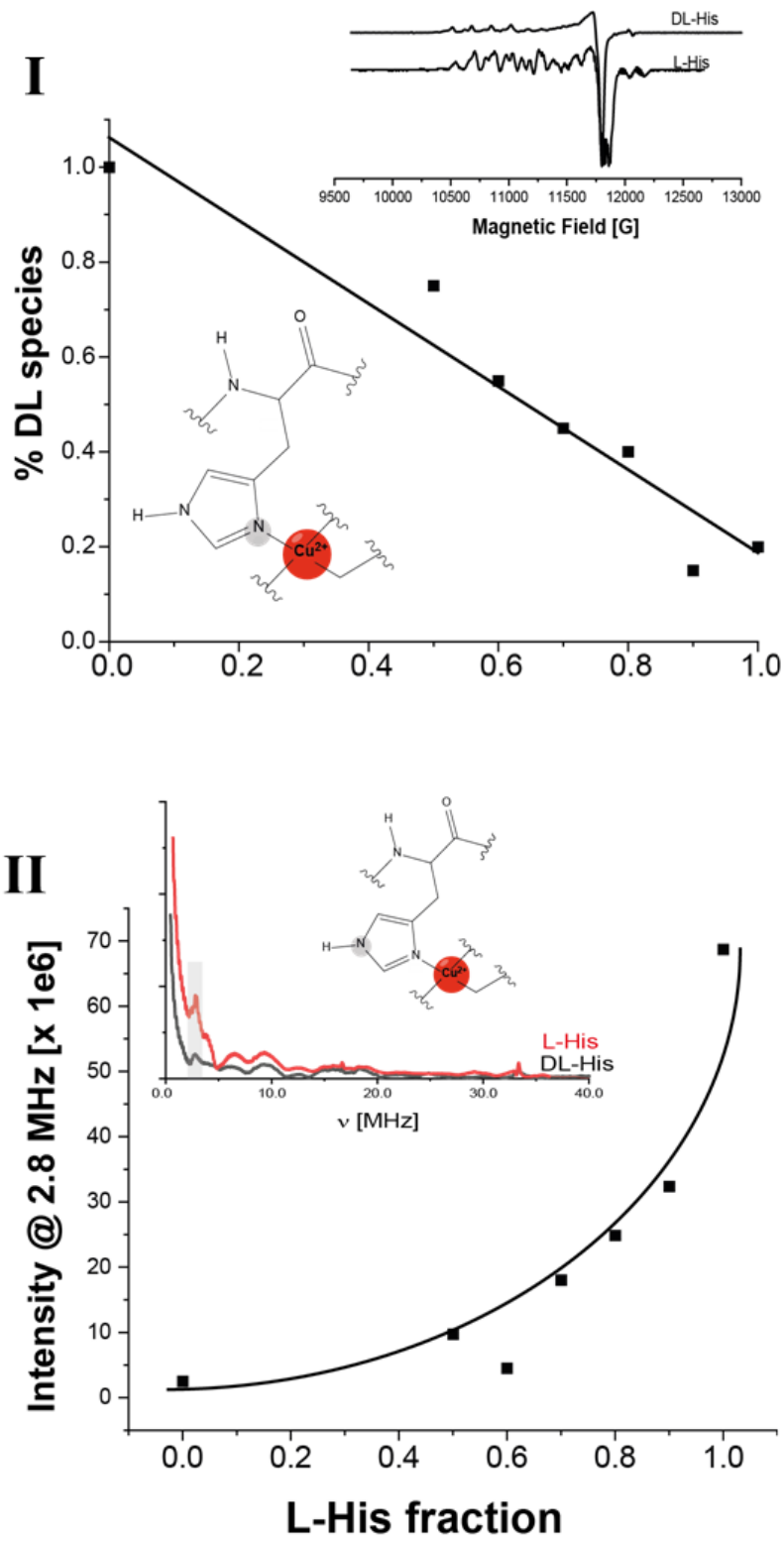

Figure 3

Chiral measurements of mixtures of Cu^{2+}-doped L/DL-His crystals: the extent of the 3O1N species detected in DL-crystal as a function of L-His concentration. The inset shows the derivative Q-band EPR spectra acquired at 20 K, 33.86 GHz for DL- and L- crystals. As well as illustration of the direct ^{14}N nuclei that are targeted by EPR measurement, R^2=0.9317 (**I**). 2.8 MHz intensity obtained from the FT spectra of the ESEEM signals. The FT spectra for the DL- and L-crystal are given in the inset. The illustration marks

the ^{14}N detected by ESEEM measurements performed at 33.86 GHz, 11790 G, with t = 220 ns, 12 ns increment, 512 points (**II**).

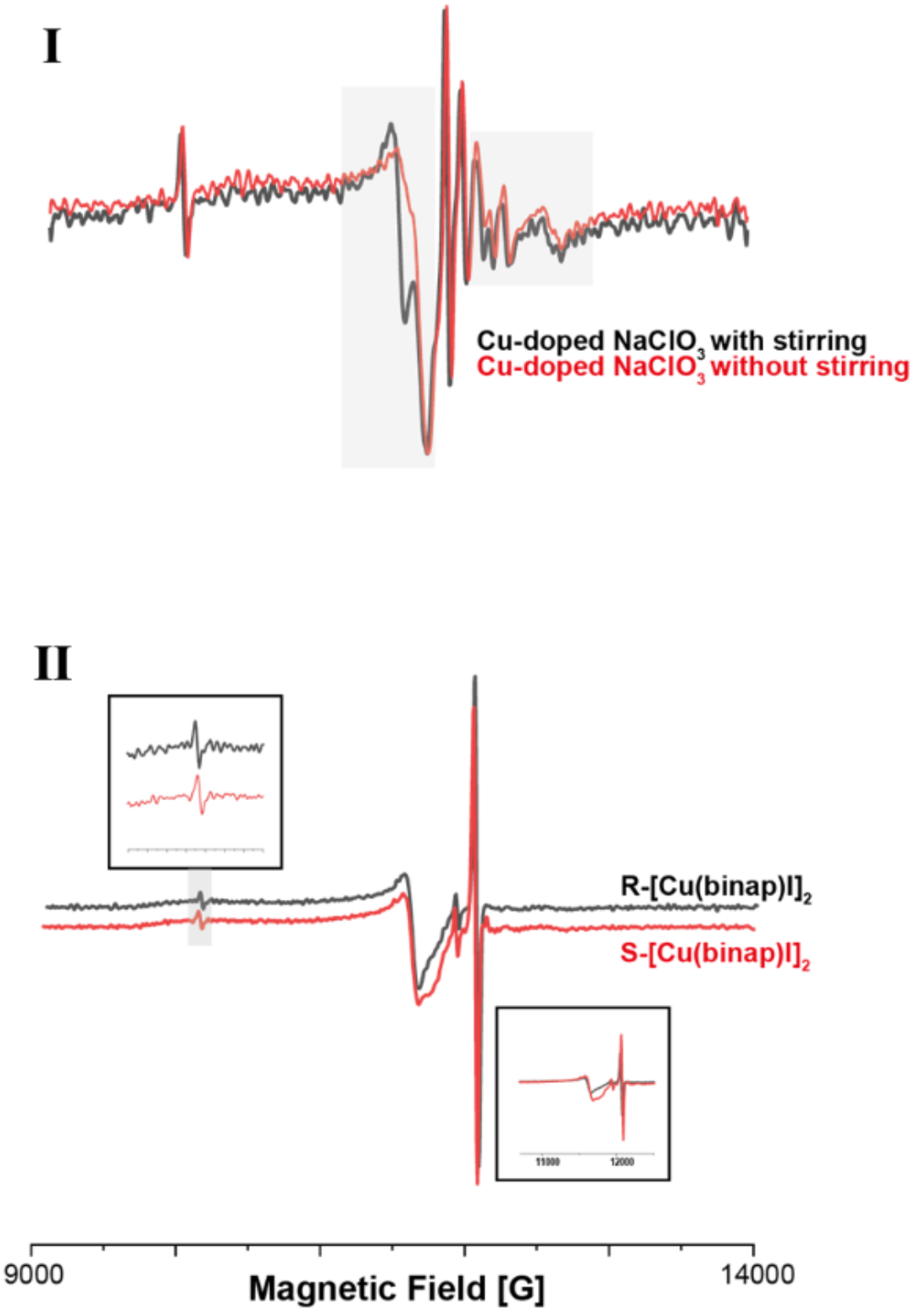

Figure 4

Q-band EPR chiral measurements of additional chiral systems: measurements of Cu^{2+}-doped $NaClO_3$ crystals with and without stirring, The gray boxes mark the changes observed between the two crystals. In

a crystal with stirring, the splitting in the $g_{\wedge}$ region is more detectable. While in the crystal without stirring, owing to inhomogeneity of the sample, this splitting is less detectable. The change in homogeneity between the two samples correlates to the change in enantiomeric excess; the sample that was stirred only contains one enantiomer therefore it is more homogeneous (**I**). And measurments of R/S - $[Cu(binap)I]_2$ crystals, Changes in splitting both in the $g_{çç}$ and $g_{\wedge}$ regions are detected between the two crystals and are manifested in the two inset boxes (**II**).

Supplementary Files

This is a list of supplementary files associated with this preprint. Click to download.

- SICuHiscommunicationsChemistryFinal.docx